Journal of Innovative Optical Health Sciences
Vol. 13, No. 3 (2020) 2030006 (20 pages)

DOI: 10.1142/S1793545820300062

Time-gated fluorescence imaging: Advances in technology and biological applications

Wenzhao Yang* and Sung-Liang Chen*,†,‡
*University of Michigan-Shanghai
Jiao Tong University Joint Institute
Shanghai Jiao Tong University
Shanghai 200240, P. R. China

†State Key Laboratory of Advanced Optical
Communication Systems and Networks
Shanghai Jiao Tong University
Shanghai 200240, P. R. China
‡sungliang.chen@sjtu.edu.cn

Received 6 November 2019
Accepted 15 January 2020
Published 14 February 2020

Time-gated (TG) fluorescence imaging (TGFI) has attracted increasing attention within the biological imaging community, especially during the past decade. With rapid development of light sources, image devices, and a variety of approaches for TG implementation, TGFI has demonstrated numerous biological applications ranging from molecules to tissues. The paper presents inclusive TG implementation mainly based on optical choppers and electronic units for synchronization of fluorescence excitation and emission, which also serves as guidelines for researchers to build suited TGFI systems for selected applications. Note that a special focus will be put on TG implementation based on optical choppers for TGFI of long-lived probes (lifetime range from microseconds to milliseconds). Biological applications by TG imaging of recently developed luminescent probes are described.

Keywords: Time-gated; fluorescence; imaging system; biological application.

1. Introduction

Fluorescence imaging, as a noninvasive imaging technique, is a versatile tool for biological and preclinical studies. It helps to observe biological processes through visualizing fluorescence signals emitted from various endogenous or exogenous fluorophores. The performance of fluorescence imaging has steady development with improved instrumentation and probes (i.e., exogenous fluorophores).[1–10] By far, fluorescence imaging is commonly based on the detection of light intensity of fluorescence emission. Ideally, the fluorescence

‡Corresponding author.

intensity indicates the localization and concentration of probes considering a simple environment (e.g., nonscattering media). However, practically, both excitation and emission intensity are affected by complicated biochemical environments (e.g., tissue absorption, scattering, and autofluorescence (AF)).[6,10] Tissue absorption limits penetration depth in tissue, and tissue scattering impairs the accuracy of the acquired localization and concentration of probes. AF can either mask desired signals or be incorrectly regarded as target signals. These factors impose intrinsic limitations on the common fluorescence imaging method. Alternatively, the detection and discrimination of fluorescence signals in the spectral or time domain offer a possible strategy to minimize the issues (e.g., AF).[10–14]

The appropriate selection of exogenous fluorophores as fluorescent probes to have different excitation and/or emission wavelengths from AF can help to obviate unwanted AF by using specific excitation wavelengths and/or filters, respectively. In the past, fluorescent probes (e.g., indocyanine green (ICG), nanoparticles (NPs), and quantum dots (QDs)) with excitation/emission wavelengths in the red or near-infrared (NIR) spectral range were employed, and the red or NIR fluorescence signal can be differentiated from AF in tissue, which commonly has excitation/emission wavelengths in the blue and green spectral range. However, unlike conventional fluorescence imaging that uses the visible wavelength range, because the excitation/emission of these NIR probes is mainly NIR light, efforts on specialized optics tailored for the NIR wavelength range (e.g., the design to minimize NIR aberrations, the choice of NIR excitation sources/detectors, etc.) is required to obtain high-quality images.[6–14] Secondly, the emission spectra from these NIR probes still overlap with AF in NIR to some extent,[3,10] which introduces crosstalk and thus degrades the image quality. Thirdly, probes such as ICG further suffer from poor stability due to being susceptible to photobleaching under long-time excitation.

Alternatively, the difference in fluorescence lifetime can be utilized as a time-resolved method to distinguish different fluorophores (e.g., probes versus endogenous fluorophores) in fluorescence imaging.[6,8–13] By using a time-gated (TG) technique, different lifetime leads to different detected fluorescence intensity, so that fluorophores with different lifetime can be distinguished. This technique is called TG fluorescence imaging (TGFI). Compared with the wavelength-resolved method, TGFI may have advantages in more flexible choices of excitation wavelengths and more effective suppression of AF. As a result, it is more likely to produce high-quality fluorescence images without much increased complexity and difficulty in building the imaging system. In this paper, we present and summarize recent advances of TGFI technology (with a special focus on TG implementation) and its biological applications. Note that the TG technique and imaging system can be utilized for all luminescent probes (i.e., not limited to fluorescent ones) once their luminescence lifetime is different from that of background. Therefore, several works on TG imaging using luminescent probes (also called TG luminescence imaging (TGLI)) are also included in this paper.

2. Principles

2.1. *Fluorescence lifetime*

Considering a simple 2-state system and assuming an excitation source with fast response time, the decay of a fluorophore molecule from an excited state to a ground state can be simply expressed as

$$I(t) = I_0 \exp(-t/\tau), \tag{1}$$

where I_0 is the initial fluorescence intensity upon excitation, and τ is the fluorescence lifetime, referring to the average time that the molecule stays in its excited state before emitting a photon. The value of τ also indicates the time when the intensity of I_0 drops to its $1/e$. Equation (1) is used without loss of generality to illustrate the decay characteristic of fluorescence signals (or more generally, luminescence signals), although the decay can be more complex for some fluorophores.[15–19] To a first approximation, fluorescence lifetime can be utilized as "labels" for different fluorophores, which can be discriminated in the time domain, as mentioned previously. In practical applications, some factors should be taken into consideration. For example, fluorescence lifetime also depends on excitation intensity to some extent, and self-quenching may occur at high fluorophore concentration.

2.2. *TG technique*

Conventionally, fluorescence imaging takes advantage of the steady-state emission intensity of

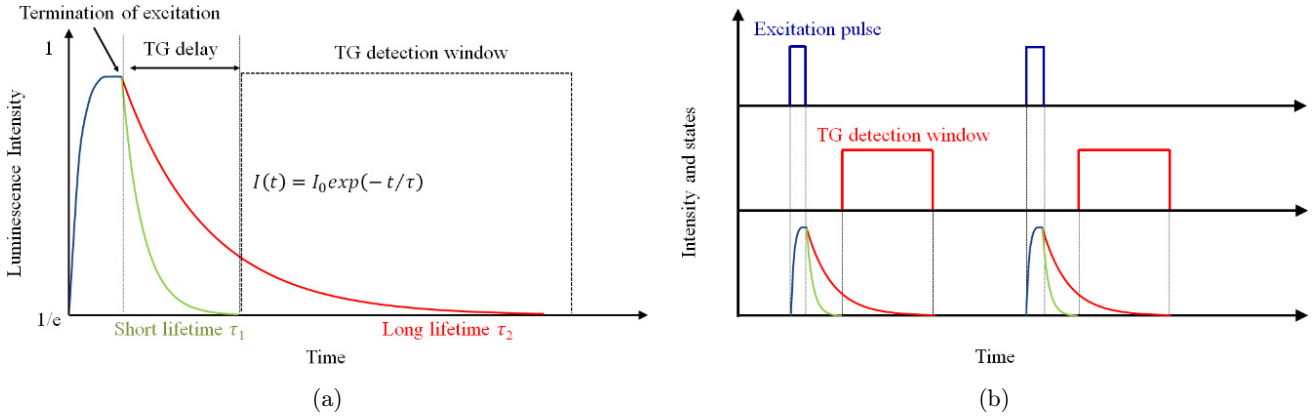

Fig. 1. (a) Illustration of TG detection in one cycle. (b) Illustration of TG detection by acquisition over multiple cycles.

fluorescent probes as the image intensity. Because continuous-wave (CW) excitation is used, this is referred to as CW imaging (in contrast to TG imaging). However, the method suffers from strong interference due to AF background that is simultaneously excited in tissue, which severely impairs the image quality, especially when very low concentration of the fluorescent probes is accumulated in the target tissue. Fortunately, TGFI technique can be utilized to overcome the issue given different fluorescence lifetime between fluorescent probes and endogenous fluorophores that produce AF background. In a typical TG imaging system, a pulsed light source can be used to excite the target probe, which usually has a comparatively long luminescence lifetime. As shown in Fig. 1(a), while long-lived luminescence signals (desired signals) are excited, short-lived luminescence signals (undesired signals) are also induced. By some means, a detector can be maintained at the off state for some time (TG delay in Fig. 1(a)). Note that in Fig. 1(a), fast termination of excitation is assumed for illustration, which is desired in practice. Then, the detection is switched to the on state (i.e., detection begins) after a suitable TG delay when the undesired signals have almost disappeared and may be switched to the off state when desired signals are mostly collected (TG detection window in Fig. 1). The above process is usually repeated for many times (i.e., acquisition over multiple cycles) to collect more desired signals from the target probe (Fig. 1(b)), and thus, signal-to-noise ratio (SNR) can be increased (more discussion below). Note that different photostability between AF and target fluorescence signals should be taken into account in practical applications. Typically, high photostability of target probes that are more resistant to photobleaching is favorable.[9] TG technique provides a novel strategy to reveal luminescent probes with high image contrast based on the use of different luminescence lifetime, which benefits many biological applications.[6,9,13,21]

In this context, background represents undesired short-lived signals (mostly AF), while noise refers to unwanted signals mainly from a detector. Compared with CW imaging, TG imaging would well increase signal-to-background ratio (SBR) (e.g., a 45-fold increase in imaging of a zebrafish embryo).[20] However, TG detection may also reject the majority of target signals, leading to low SNR, which could possibly be improved by signal averaging (i.e., acquisition over multiple cycles), given good photostability as mentioned previously, at the expense of acquisition time.

3. Instrumentation and Methodology

3.1. *Excitation*

Excitation of fluorescence (or in general, luminescence) signals can be achieved by light sources including lamps, light-emitting diodes (LEDs), or lasers. The choice of excitation wavelength is largely dependent on the target fluorophore. For example, many lanthanide-based probes that emit luminescence signals by excitation in the UV, violet, or blue spectral range have large Stokes and/or anti-Stokes shifts, and long luminescence lifetime (tens of microseconds to several milliseconds).[9,21–24] Terbium ions (Tb^{3+}) are typically excited at wavelength of ~320 nm. Europium ions (Eu^{3+}) excitation spectrum is ~337–370 nm. Ytterbium ions (Yb^{3+})

also emit fluorescence signals with UV excitation. Besides, in recent years, many nano-scaled long lifetime fluorescent probes (e.g., NPs and QDs) have been shown to provide a flexible choice of excitation wavelength in the range from UV to NIR.[4,5,8–10,25]

Due to long warm-up time and extinguishing time, lamp-based excitation sources are rarely used in TG imaging that requires precise and rapid modulation of the illumination. With the development of LEDs and lasers, they can be rapidly switched on and off, and the switching time scale can be much shorter than the luminescence lifetime of most long-lived probes. Besides, LEDs and lasers provide more stable illumination intensity, and the intensity is strong enough to excite sufficient fluorescence signals. Therefore, LEDs and lasers are suitable light sources for TG imaging and have been adopted in TG imaging systems.[11,20,24–52]

To enable imaging of a variety of luminescent probes, different excitation wavelengths are required and can be equipped using multiple LED/laser sources with increased cost, and complexity of imaging systems. Alternatively, one excitation source with tunable wavelengths offering a certain range of excitation wavelengths can be employed, which is supposedly simpler for imaging system implementation. Tunable wavelengths can be achieved by integrating filters or gratings with lamps or by using commercial tunable lasers.

Comparison of excitation sources including lamps, LEDs, CW lasers, and pulsed lasers for TG imaging is provided in Table 1. In general, for excitation sources, tunable wavelengths facilitating excitation of more types of probes, laser pulses with easy implementation and short duration, good power stability, good quality of beam focusing, and low cost are desired.

3.2. *Detection*

Single-pixel-based detectors such as single-photon avalanche diodes (SPADs) and photomultiplier tubes (PMTs) are widely used in fluorescence detection, and they offer high sensitivity with a large dynamic range, yet the imaging speed is usually limited by point-by-point scanning. Note that SPAD array and multianodes PMT[53,54] detectors are categorized as array detectors (described below). On the other hand, array detectors mainly including charged coupled device (CCD), intensified CCD (ICCD), electron multiplication CCD (EMCCD), and complementary metal-oxide-semiconductor (CMOS) sensors are able to render fluorescence images by one-shot acquisition, which is favorable for fast and real-time imaging. CCD and CMOS sensors convert photons into electrons on chips without amplifying the number of electrons upon the conversion, and acquisition over multiple cycles is typically used to increase SNR. For TG imaging, CCD and CMOS sensors can be integrated with an optical chopper for the TG implementation (described later). As for ICCD, it has an array for photo multiplication before coupling to a CCD sensor, and thus functions as an image intensifier to provide gain for the CCD. Besides, the intensifier can be rapidly switched on/off to facilitate TG detection. As for EMCCD, it is able to detect single photon events by an electron multiplier. For TG imaging, ICCD and EMCCD combined with either an electronic unit or an optical chopper for synchronization are used to realize the TG implementation (described later), which provides high sensitivity because of the gain. Besides, during the past decade, time-resolved SPAD and PMT array detectors, including commercial ones, were developed and applied in TG imaging.[39,55–60]

Table 1. Comparison of excitation sources for TG imaging.

	Wavelength		Pulse				
Excitation source	Bandwidth	Tunability	Implementation	Duration	Power stability	Quality of beam focusing	Cost
Lamp	Wide	Yes[a]	Hard	Long	Bad	Bad	Moderate
LED	Moderate	No	Moderate	Short	Moderate	Moderate	Low
CW laser	Narrow	Depends[b]	Moderate	Short	Good	Good	Low[b]
Pulsed laser	Narrow	Depends[b]	Easy	Shortest	Good	Good	High[b]

Notes: [a]By filters or gratings.
[b]Higher cost for tunable lasers compared with single-wavelength counterparts.

Table 2. Comparison of detectors for TG imaging.

Detector	Pixel	Sensitivity	Typical TG implementation	Cost
SPAD	Single/array	Very high[a]	Electronic unit	Moderate
PMT		Very high		High
CCD		Moderate	Optical chopper	Low
CMOS	Array	High		Low
ICCD		High	Electronic unit[b]; optical chopper	High
EMCCD		High		High

Notes: [a]For visible wavelength range.
[b]ICCD or EMCCD combined with electronic units for synchronization provides the fastest response for TG implementation.

Comparison of detectors for TG imaging is provided in Table 2. Overall, ICCD/EMCCD has higher sensitivity than CCD, while the latter is cheaper. With the advances of CMOS technology, CMOS cameras are becoming sensitive and suitable for TG imaging applications. The high fluorescence signal intensity is always desired for good image quality. TG detection based on optical choppers and electronic units for synchronization is described in Secs. 3.3 and 3.4, respectively. In recent years, commercial TG imaging systems based on the above-mentioned detectors have been developed and applied.

Besides the six detectors for TGFI mentioned above, there are a few other variant detectors or detection technologies developed for TG imaging and detection. Hybrid photodetectors, such as GaAsP hybrid photomultipliers and InGaAs emICCD, were also used for TG imaging.[25,51,61,62] Current-assisted photonic sampler arrays combined with CMOS sensors were developed for TG detection.[63] Time-correlated single photon counting (TCSPC) technique based on SPAD or PMT detectors was used in TG imaging.[13,29,39,47] In addition, various fluorescence imaging and detection based on TG technique was also demonstrated, including fluorescence lifetime imaging (FLIM),[13,26,43,47,64–66] TG Förster resonance energy transfer (FRET),[40,67–69] and fluorescence diffuse optical tomography.[33]

3.3. *TG implementation based on optical choppers*

Optical choppers, together with either CW or pulsed excitation sources, can be used to realize TG detection. In terms of synchronization for the TG implementation, there are mainly four schemes: (i) Chopper sensor signals to synchronize excitation, (ii) Two phase-locked choppers to synchronize excitation/detection, (iii) A controller/function generator to synchronize excitation with a chopper, (iv) Spatial alignment of excitation/emission beam spots for synchronization. They are denoted as OC-(i), OC-(ii), OC-(iii), and OC-(iv), respectively. The working principles and examples are described below.

OC-(i) is illustrated in Fig. 2. An excitation beam is used to excite luminescence signals, and the emission beam is modulated by an optical chopper before entering a detector. A chopper sensor is used to carry the transmission/blocking information of the chopper and thus the on/off status of the detection, as shown in the green pulse train in Fig. 2. Note that the chopper sensor can be placed at a suitable position to have the same phase as the emission beam, as shown in the green and red pulse trains in Fig. 2. Then, the green pulse train and a delay unit (with a proper delay time (Fig. 2)) can be used to trigger and synchronize the excitation beam, as shown in the blue pulse train in Fig. 2, so that a proper TG delay can be realized. Note that

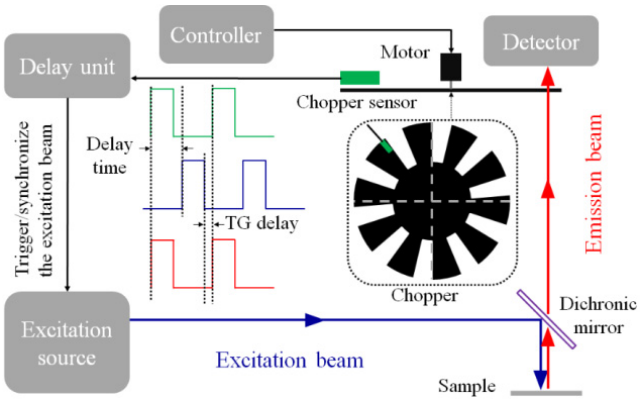

Fig. 2. TG implementation of OC-(i).

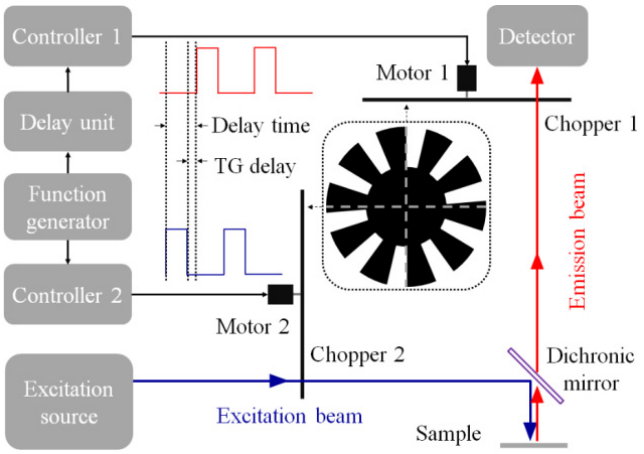

Fig. 3. TG implementation of OC-(ii).

the chopper's duty cycle has to be $< 50\%$ (i.e., transmission $<$ blocking) so that the TG delay can be possible. As an example, Beverloo *et al.* built a TG imaging system by modifying an epi-fluorescence microscope equipped with a Xenon flash lamp.[70]

OC-(ii) is illustrated in Fig. 3, where two optical choppers are used. Instead of using a chopper sensor, a function generator is used to actively modulate the excitation and emission beams (by blue and red pulse trains, respectively, in Fig. 3) with a proper delay time via a delay unit. As an example, Marriott *et al.* adopted two choppers for TG imaging.[11,23]

OC-(iii) is illustrated in Fig. 4. Similar to OC-(ii), active modulation of the excitation and emission beams are used. A chopper is used to modulate the emission beam, which is the same as OC-(ii). As for modulating the excitation beam, instead of using

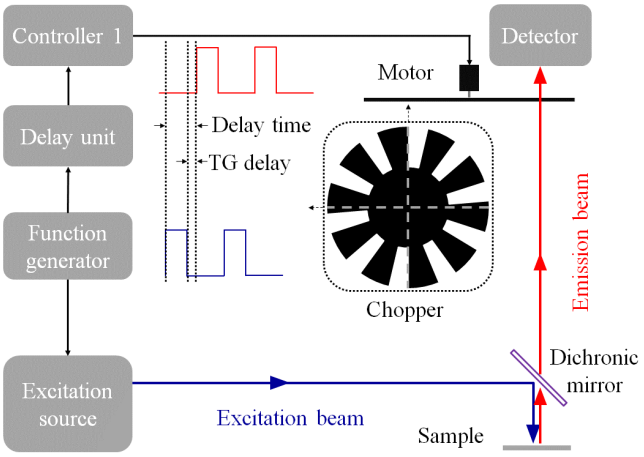

Fig. 4. TG implementation of OC-(iii).

Chopper 2 as used in OC-(ii), electronic modulation is adopted. Similarly, synchronization and a proper TG delay can be achieved. Several works based on OC-(iii) were reported.[12,32,37,48,71,72] Jin *et al.* demonstrated a low-cost implementation of a TG imaging system (Fig. 5(a)) allowing direct visual inspection of stained samples.[32] In this system, the UV LED as pulsed excitation was synchronized by the clock signal from a chopper controller. Zheng *et al.* and Zhang *et al.* also demonstrated TG imaging by OC-(iii) using a chopper controller.[37,71] Very recently, Cheng *et al.* have implemented a TG imaging system with the synchronization by OC-(iii) using an arbitrary waveform generator.[48] As shown in Fig. 5(b), the waveform generator outputs TTL signals, which are synchronized with the chopper at the same frequency are used to synchronize the laser source. Ratiometric detection was demonstrated based on the collection of two luminescent signals with the same emission wavelength which can be utilized to minimize interferences from photon attenuation in tissue and thus facilitates accurate *in vivo* detection. Gu *et al.* realized high-sensitivity TG imaging of NIR probes in a tumor-bearing mouse model, and the system was also based on OC-(iii) using an arbitrary waveform generator.[51]

OC-(iv) is illustrated in Fig. 6, which has been reported very recently.[20,44,45,52] Different from other optical-chopper-based TG methods (OC-(i), OC-(ii), and OC-(iii)) that use delay units and TTL signals for synchronization, OC-(iv) employs a single optical chopper and spatial alignment of the excitation/emission beam spots with the chopper, which leads to a fixed phase difference between the excitation and detection (blue and red pulse trains, respectively, in Fig. 6(a)) for synchronization in TG detection. In this regard, the TG delay is determined by chopper-related parameters including the rotation speed and duty cycle of the chopper, etc. Similarly, the chopper's duty cycle has to be $< 50\%$ so that the TG delay can be realized. The working principle is shown in Figs. 6(b) and 6(c). As shown in Fig. 6(b), excitation and emission beam spots (blue and red crosses, respectively) are precisely aligned with the chopper. During TG image acquisition, the chopper is rotating while the two beam spots are kept stationary. In a TG acquisition cycle, four on/off switches of excitation/emission occur, which are denoted as T1, T2, T3, and T4 in Figs. 6(b) and 6(c). The period of T1 and T2 determines the excitation duration, that of T2 and

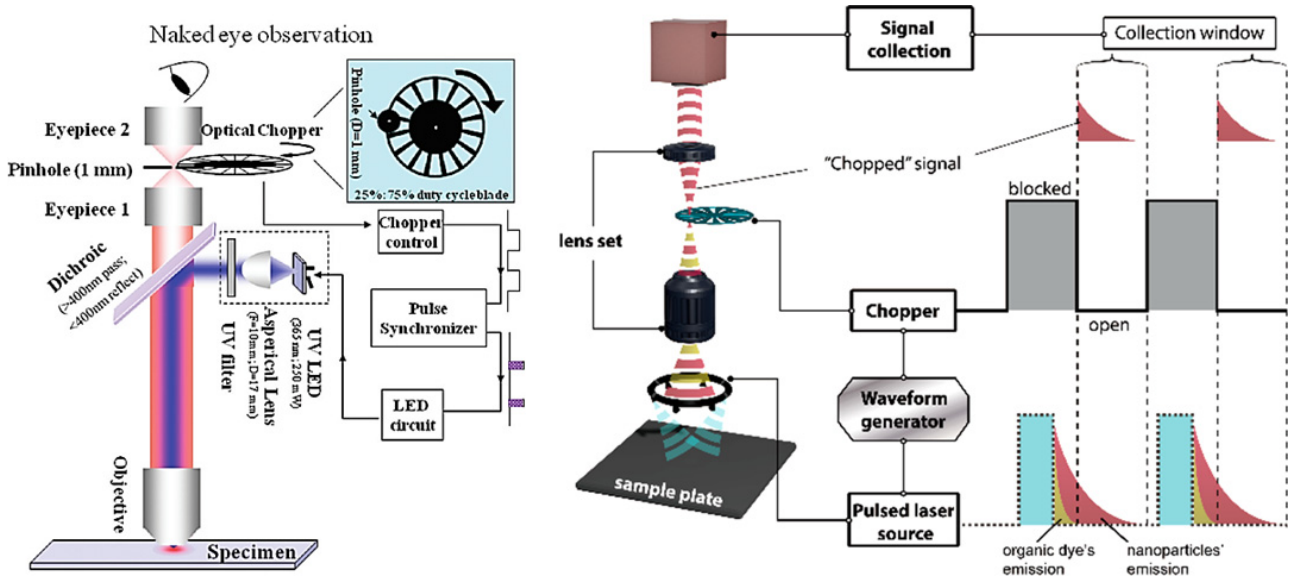

Fig. 5. Example of OC-(iii). (a) Synchronization output was provided by the clock signal from the chopper controller, producing TTL signals to trigger the UV LED circuit, so that an appropriate TG delay can be achieved. (b) Synchronization output was provided by the waveform generator, producing TTL signals that were synchronized with the chopper and were used to synchronize the laser source. An appropriate TG delay can be achieved by setting parameters such as the duty cycle and the initial phase of the TTL signals. Reprinted with permission from Refs. 32 and 48.

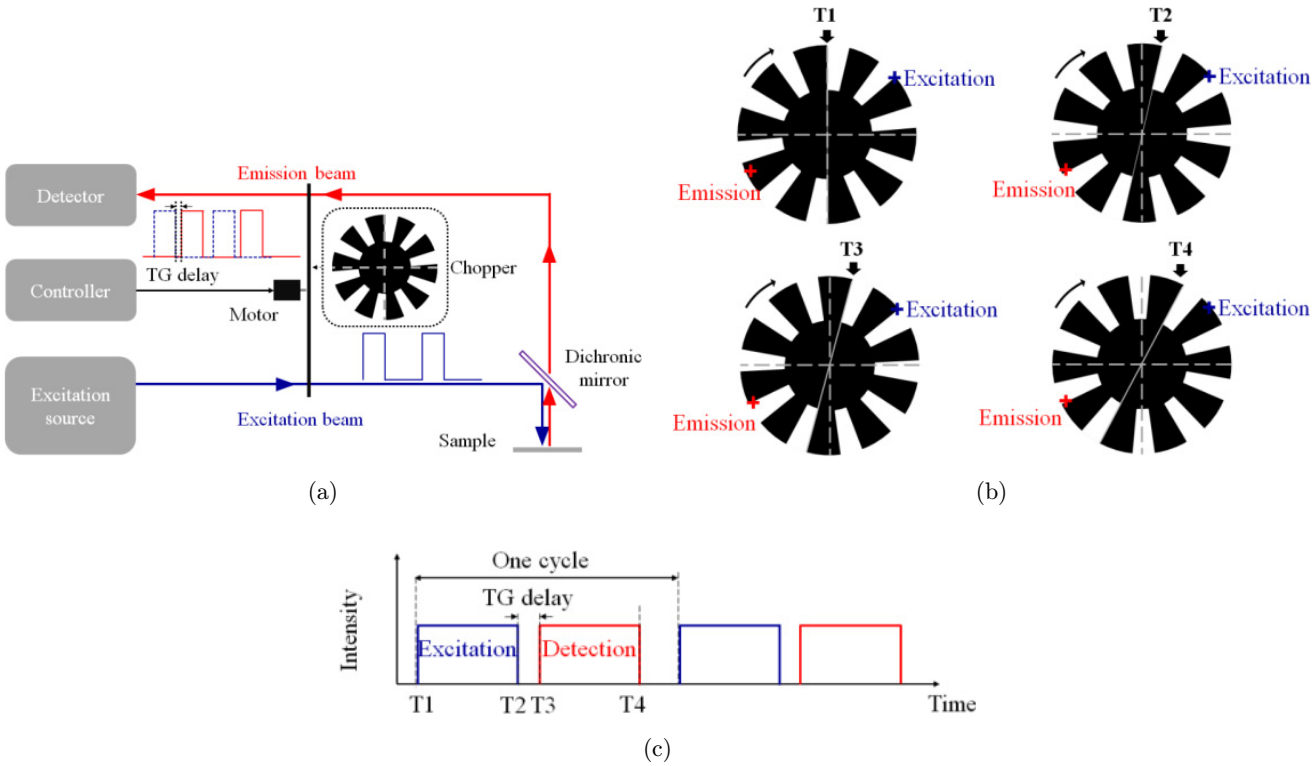

Fig. 6. (a) TG implementation of OC-(iv). (b) Illustration of the spatial alignment of the excitation and emission beam spots with the chopper. When the chopper is rotating, four on/off switches of excitation/emission occur and are denoted as T1, T2, T3, and T4. (c) Excitation duration and TG detection window in a TG acquisition cycle. Note that the beam spots are assumed to be infinitely small. A phase difference between the excitation and detection is achieved by virtue of the spatial alignment mentioned in (b), and thus, TG detection is realized.

T3 the TG delay, and that of T3 and T4 the TG detection window. Sakiyama *et al.* demonstrated TG imaging in the NIR-II range based on OC-(iv).[44] Further, Zhu *et al.* utilized the OC-(iv) approach for TG detection and demonstrated the applications including TG luminescence spectra measurement and fast luminescence lifetime imaging.[45,52] Our group also built a system based on OC-(iv).[20] Using the system, we demonstrated high-contrast TGFI of long-lived silicon (Si) QD NPs microinjected into zebrafish embryos and larvae.

Alternatively, a variant of OC-(iv) employs a single reflective rotor to realize TG implementation, which is termed as a gated autosynchronous luminescence detector (GALD) firstly reported by Connally *et al.*[73] Similar to OC-(iv), different positions of the rotor define the excitation duration, TG delay, and TG detection window in a TG acquisition cycle. A remarkably small footprint of the GALD enables its insertion into the differential contrast prism of an Olympus microscope.[73]

Table 3 is a summary of TG implementation based on optical choppers. Note that low-cost excitation sources (lamps, LEDs and CW lasers) were used in these works. Overall, the optical-chopper-based method provides a convenient and low-cost approach for TG imaging mainly because cheap light sources (e.g., lamps, LEDs, or CW lasers) and detectors (e.g., CCD or CMOS) are required. However, the switching time of excitation/detection using optical choppers is inherently slower than using electronic units.

3.4. *TG implementation based on electronic units*

TG methods based on electronic units refer to the TG delay realized or modulated purely by electronic units (i.e., without any mechanical modulation), such as a purely-electronic delay circuit or an optical fiber delay line to synchronize with an electronic delay. Similarly, the SNR can be further enhanced by acquisition over multiple cycles at the expense of imaging speed. In terms of synchronization for the TG implementation, there are mainly three schemes: (i) An optical fiber delay line to synchronize with an electronic delay, (ii) A purely-electronic delay circuit (e.g., using a function/waveform generator), (iii) A TCSPC module. They are denoted as EU-(i), EU-(ii), and, EU-(iii), respectively. The examples and brief working principles are described below.

Table 3. Summary of TG implementation based on optical choppers.

TG implementation	Detection	Ref.
OC-(i)	CCD	70
OC-(ii)	CCD	11, 23
OC-(iii)	CCD	32, 71, 72, 74–77
	ICCD	12, 51
	EMCCD	37, 48
OC-(iv)	CCD	44, 45, 52
	CMOS	20
	GALD	73, 78

For EU-(i), Wang *et al.* used a pulsed laser for excitation and a gated image intensifier for the TG detection window.[26] For excitation, an optical fiber delay line was used to realize a delayed laser pulse, while for detection, a digital delay pulse generator was utilized to determine the beginning of the TG detection window. In this regard, the optical fiber delay line can be utilized to synchronize the excitation with the delayed detection by the gated image intensifier, and a TG delay of several nanoseconds can be achieved. Cubeddu *et al.* also demonstrated TG imaging based on EU-(i).[27]

For EU-(ii), Valentini *et al.* used ICCD for the TG detection window, which was synchronized with laser pulses by a passive delay generator, and the TG delay can be realized.[28] Gahlaut *et al.* also used a delay generator to output TTL pulses to synchronize an LED and ICCD, and the TG delay was programmable by the delay generator.[79] TG imaging of living cells was demonstrated. Lu *et al.* demonstrated a catheter for NIR fluorescence/OCT imaging, where the TG imaging was realized by using a custom-made delay chip to adjust the TG delay between the excitation laser pulse and SPAD detection.[19] Bouccara *et al.* utilized two phase-locked function generators to synchronize a pulsed laser diode and an intensifier (of EMCCD) for AF rejection.[34] Pons *et al.* also used EU-(ii) for *in vivo* imaging of single tumor cells in fast-following bloodstream.[49] Sreenivasan *et al.* built a TG imaging system that was synchronized by dual TTL signals, which were used to modulate the laser source and EMCCD to achieve the desired TG delay and TG detection window.[42]

For EU-(iii), Dahan *et al.* utilized a scanning controller board to output a TTL pulse, which was used to trigger the acquisition of fluorescence

Table 4. Summary of TG implementation based on electronic units.

TG implementation	Detection	Ref.
EU-(i)	ICCD	26, 27
EU-(ii)	ICCD	28, 30, 31, 35, 30, 43, 51, 79
	SPAD	19
	EMCCD	24, 34, 36, 42, 49
EU-(iii)	TCSPC module	29, 39, 41, 47, 50, 80

photons by a TCSPC card.[20] Chen *et al.* and Tu *et al.* demonstrated TG fluorescence detection for high-contrast quantum imaging and TG imaging of labeled live cancer cells, respectively, based on EU-(iii).[39,50]

Table 4 is a summary of TG implementation based on electronic units. Note that pulsed (or electronically-modulated) laser illumination was used in these works. In TG acquisition, to capture maximum luminescence signal intensity so as to optimize image quality, a minimum TG delay that ensures complete suppression of AF background is required. To achieve this, the excitation has to be quickly switched off (e.g., $< 1/10$ of the lifetime of a target probe), and meanwhile, the TG delay has to be sufficiently short (e.g., $<$ the lifetime of the target probe), but not shorter than the above-mentioned minimum TG delay. In this regard, electronic-unit-based methods generally perform better than optical-chopper-based methods. Further, among electronic-unit-based methods, EU-(iii) attains the highest time resolution (tens of picoseconds) and well succeeds in selected applications that intend to capture TG images of target probes with very short lifetime.

4. Biological Applications

TGFI relies on the detection of fluorescence signals taken with a time delay after the excitation is switched off. Benefited by years of development of lasers, imagers, and long-lived fluorescent probes as markers, TGFI has made great technical progress in recent years. Further, FLIM technique is able to produce lifetime maps, which is basically implemented by gradually adjusting the TG delay.[13,26,43,47,64–66] TCSPC is one of the main approaches to realize FLIM. TGFI has been widely utilized in many biological and medical applications. In this section, we present TGFI applications to the objects at a multiple length scale from molecules to tissues. As mentioned previously, some works on TGLI applications using luminescent probes are also included.

The importance of the choice of the luminescent probes used as labels in TG imaging cannot be overemphasized.[21,22] The parameters of probes (e.g., high quantum yield and proper lifetime), good labeling, and no or little quenching are key factors to render high-quality images in TG imaging applications.

Depending on the luminescence lifetime of the target probe, one may choose proper instrumentation for TG imaging. For quite long luminescence lifetime (e.g., lanthanide-based probes) up to millisecond time scale,[32,71,72,74,76,78,81] simple and low-cost instrumentation (mainly optical-chopper-based methods) is well satisfactory. By contrast, for quite short luminescence lifetime down to nanosecond time scale,[28,29,31,33,34,47,66] complex and expensive instrumentation (mainly electronic-unit-based methods) must be employed.

A summary of biological applications, used luminescent probes, and employed TG instrumentation is provided in Table 5.

4.1. *Molecules, cells, and microorganisms*

Recovery of the concealed micro objects such as large molecules,[11,28] cells,[11,23,29,34,36,39,41,47,49,66,70,72,74–84] and microorganisms[24,30,32,71,85] from annoying interference (e.g., background AF) in fluorescence imaging with the help of TG technique has attracted increasing attention for years.

Marriott *et al.* presented a simple TG microscope and utilized it to visualize the delayed luminescence intensities and lifetime of acridine dyes on polytene chromosomes.[10] Valentini *et al.* utilized TGFI for DNA-microarray reading.[28] The TGFI system employed an ICCD camera with picosecond resolution to acquire time-delayed fluorescence images, which were used to calculate the amplitude map of the marker, cyanine 3. As shown in Fig. 7, DNA microarray marked by cyanine 3 is clearly distinguished from the background by TGFI (Fig. 7(b)).

In cellular biology, long-lived fluorescent probes serve as useful markers to study cell morphology and function. To effectively image the long-lived fluorescent probes, TG detection is used to eliminate interference from cellular AF. In 1990,

Table 5. Summary of biological applications, used luminescent probes, and employed TG instrumentation.

Biological application		Luminescent probe		TG instrumentation			
Category	Sample	Probe	Lifetime	TG implementation	Excitation	Detection	Ref.
Molecule	Polytene chromosome	Acridine orange	∼1 ms	OC-(ii)	CW laser	CCD	11
	DNA microarray	Cyanine 3	2.1 ns	EU-(ii)	Pulsed laser	ICCD	28
Cell	3T3 cell	Acridine orange	∼1 ms	OC-(ii)	CW laser	CCD	11
	D. discoideum cell	SBMC	∼740 μs	OC-(ii)	Lamp	CCD	23
	3T3 cell	CdSeZnS QD	Tens of ns	EU-(iii)	Pulsed laser	TCSPC	29
	HeLa cell	Zn–Cu–In-Se/ZnS core/shell QD	150 ns	EU-(ii)	Pulsed laser	EMCCD	34
	AtT20 cell	Nanoruby	3.7 ms	EU-(ii)	CW laser	EMCCD	36
	SKOV cell	SiQD-NP	25 μs	EU-(iii)	Pulsed laser	TCSPC	39
	HeLa cell	Cpy-Odot	9.3 μs	EU-(iii)	Pulsed laser	TCSPC	41
	AtT20 cell	NeutrAvidin-coupled nanoruby	∼4 ms	EU-(ii)	CW laser	EMCCD	42
	DU-145 cell	HA-ADOTA	17 ns	EU-(iii)	Pulsed laser	TCSPC	47
	A20 lymphoma cell	ZnCuInSe/ZnS QD	150.−300 ns	EU-(ii)	Pulsed laser	EMCCD	49
	SK-BR-3 cell	CIS/ZnS QD	21 ns	EU-(iii)	Pulsed laser	TCSPC	66
	Human erythrocyte and lymphocyte	Phosphor	700 μs	OC-(i)	Lamp	CCD	70
	HepG2 cell	TOB-Eu^{3+}	180 μs	OC-(iii)	Lamp	CCD	72
	MDCKII cell	Lumi4-Tb	∼600 μs	EU-(ii)	LED	ICCD	79
	DU-145 cell, C3 cell	BHHBTEGSB	∼300 μs	OC-(iv)	LED	GALD	78
	Raw 264.7 cell	BHHBB–Eu^{3+}	∼600 μs	EU-(iii)	Lamp	TCSPC	82
	Raw 264.7 cell, HepG2 cell	BHHBCB-Eu^{3+}	∼600 μs	EU-(iii)	Lamp	TCSPC	83
	HeLa cell, HepG2 cell, MCF-7 cell	Ru-2	Hundreds of ns	EU-(iii)	Lamp	TCSPC	84
	Raw 264.7 cell	Mito-NPSTTA-Eu^{3+}	∼1 ms	OC-(iii)	Lamp	CCD	74
	HepG2 cell	TRP-NO	Tens to hundreds of μs	OC-(iii)	Lamp	CCD	75
	HepG2 cell	Eu^{3+}-BHHCT-BPED	∼800 μs	OC-(iii)	Lamp	CCD	76
	HEK293 cell	Carbon-bridged dye	16 ns	EU-(iii)	—	TCSPC	80
	Raw 264.7 cell	PTTA-Eu^{3+}-CoFeO-FA NP	Several ms	OC-(iii)	LED	CCD	77
	HeLa cell	BHHBB–Eu^{3+}@MnO2 NP	530 μs	OC-(iii)	Lamp	CCD	81
Microorganism	Giardia lamblia cyst	BHHST	>500 μs	EU-(ii)	LED	EMCCD	24
	Giardia lamblia cyst	BHHST	>500 μs	EU-(ii)	LED	ICCD	30
	Giardia lamblia cyst	Eu3+ luminescence bead	>500 μs	EU-(ii)	LED	ICCD	85

Table 5. (*Continued*)

Biological application		Luminescent probe		TG instrumentation			
Category	Sample	Probe	Lifetime	TG implementation	Excitation	Detection	Ref.
	Giardia lamblia cyst, Cryptosporidium parvum oocyst	BHHCT-europium complex	$>100\,\mu s$	OC-(iii)	LED	CCD	32
	Giardia lamblia cyst, Cryptosporidium parvum oocyst	$Y_2O_2S:Eu^{3+}$ NP	Hundreds of μs	OC-(iii)	Lamp	CCD	71
	Daphnia magna	BHHBB–Eu^{3+}	$\sim 600\,\mu s$	EU-(iii)	Lamp	TCSPC	82
	Daphnia magna	BHHBCB-Eu^{3+}	$\sim 600\,\mu s$	EU-(iii)	Lamp	TCSPC	83
	Daphnia magna	Ru-2	Hundreds of ns	EU-(iii)	Lamp	TCSPC	84
Tissue	Zebrafish model	Cpy-Odot	$9.3\,\mu s$	EU-(iii)	Pulsed laser	TCSPC	41
	Zebrafish model	SiQD-NP	$25\,\mu s$	OC-(iv)	CW laser	CMOS	20
	Zebrafish model	BHHBB–Eu^{3+}	$\sim 600\,\mu s$	EU-(iii)	Lamp	TCSPC	82
	Zebrafish model	Mito-NPSTTA-Eu^{3+}	~ 1 ms	OC-(iii)	Lamp	CCD	74
	Zebrafish model	BHHBB–Eu^{3+}@MnO2 NP	$530\,\mu s$	OC-(iii)	Lamp	CCD	81
	Mouse model	Hematoporphyrin derivative	15 ns	EU-(i)	Pulsed laser	ICCD	27
	Mouse model	CSQD	>20 ns	EU-(ii)	LED	ICCD	31
	Mouse model	PSiNP	$60\,\mu s$	EU-(ii)	LED	ICCD	35
	Mouse model	NdNP	$\sim 100\,\mu s$	EU-(ii)	Pulsed laser	InGaAs emICCD	25
	Mouse model	UCNP	Hundreds of μs to several ms	OC-(iii)	Pulsed laser	EMCCD	37
	Mouse model	CIS/ZnS QD	Tens to hundreds of ns	—	—	—	38
	Mouse model	$NaYF_4$:Nd	$53\,\mu s$	OC-(iii)	CW laser	EMCCD	48
	Mouse model	$NaYbF_4$@CaF_2	2.19 ms	EU-(ii)	Pulsed laser	InGaAs emICCD	51
	Mouse model	BHHBB–Eu^{3+}@MnO2 NP	$530\,\mu s$	OC-(iii)	Lamp	CCD	81
	Mouse model	LPSiNP	5–$13\,\mu s$	—	—	—	86
	Human tonsil tissue	Lumi4tb-Tyr	>2 ms	EU-(ii)	LED	ICCD	40

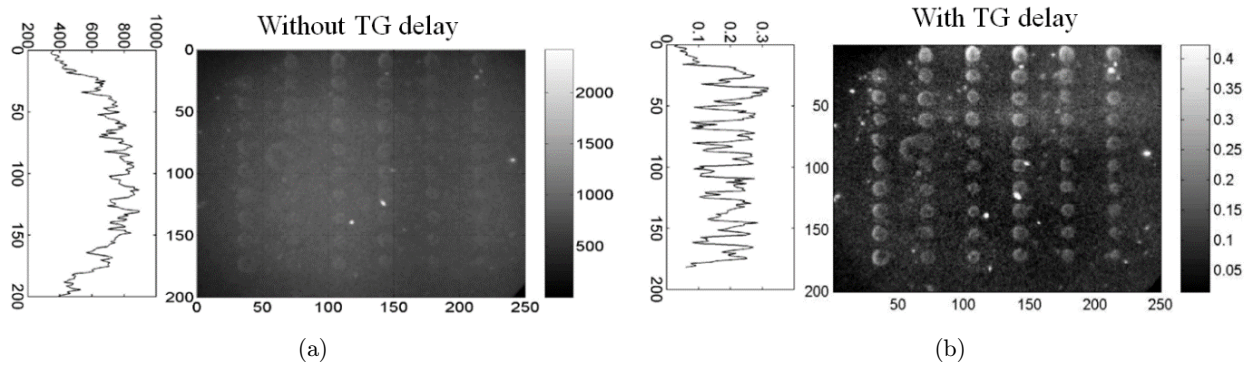

Fig. 7. Fluorescence images of DNA microarray marked by cyanine 3. (a) The image was taken synchronously with the excitation pulses. (b) The image was taken with a set of time delays, and the amplitude map of cyanine 3 can be calculated. The line profiles across the first column of the DNA microarray images are shown at left in (a) and (b), respectively. Reprinted with permission from Ref. 29.

Beverloo *et al.* presented inorganic phosphors with delayed luminescence.[70] Visualization of human lymphocytes labeled with the inorganic phosphors by TG imaging was demonstrated. Background AF suppressed by at least two orders of magnitude was achieved. One year later, Marriott *et al.* reported visualization of 3T3 cells stained with acridine dyes by TG imaging, and particular cellular structures became obvious by the ratio image (phosphorescence/fluorescence).[11] In the last decade, TG

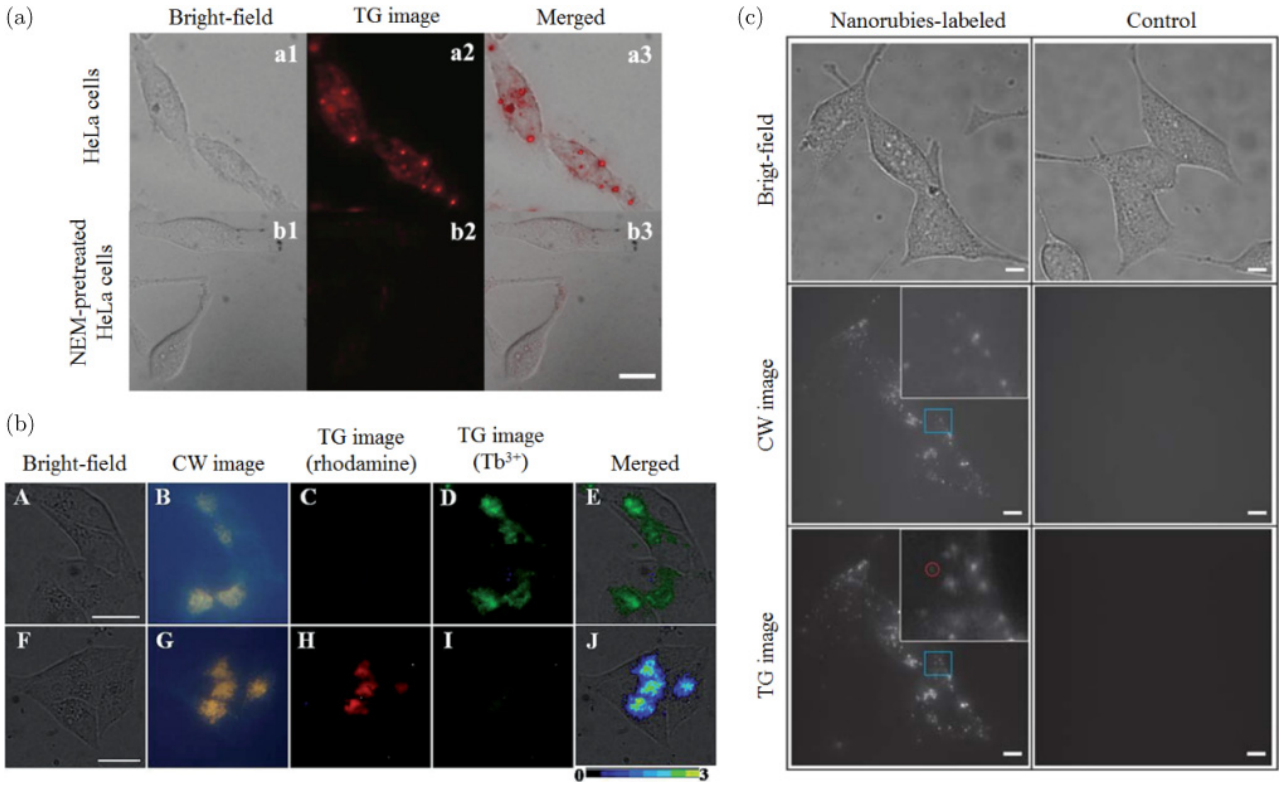

Fig. 8. (a) Images of HeLa cells (top) and NEM-pretreated HeLa cells (bottom, as control experiment) incubated with BHHBB–Eu^{3+}@MnO_2 for 3 h (1: bright-field images; 2: TG images; 3: merged images of 1 and 2). Scale bar: 10 μm. (b) Bright-field (A and F), CW (B and G), and TG (C and H for rhodamine luminescence, and D and I for Tb^{3+} luminescence) images of the TRP-NO-loaded HeLa cells before (top) and after (bottom) incubation with nitric oxide. Image E is the merged image of A and D, and image J is the merged image of F and a ratiometric (ratio = H/I) luminescence image. Scale bar: 10 μm. (c) Bright field, CW, and TG images of AtT-20 cells incubated with nanorubies (left column) and control (right column), respectively. Scale bar: 10 μm. Reprinted with permission from Refs. 36, 75, and 81.

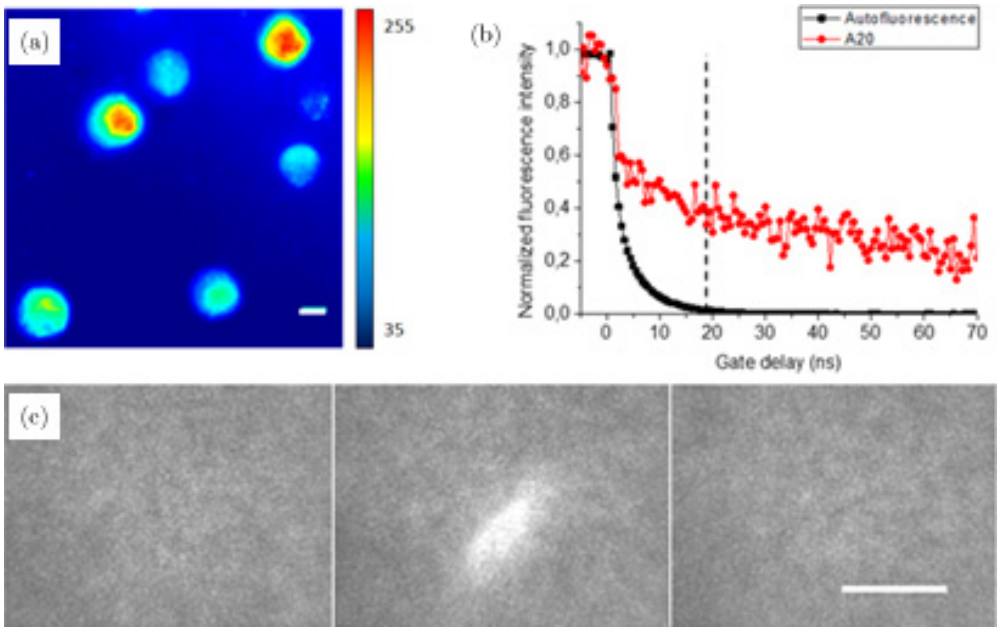

Fig. 9. TG imaging of QD-labeled A20 tumor cells in a rat bloodstream. (a) Classical epi-fluorescence microscopy image (CW imaging) of the cells. Scale bar: 5 μm. (b) The AF (black) and fluorescence of the QD-loaded A20 cells (red) as a function of TG delay. (c) Three consecutive *in vivo* TG fluorescence images showing a QD-labeled A20 cell flowing in a blood vessel. Scale bar: 50 μm. Reprinted with permission from Ref. 49.

imaging of living cells has been extensively demonstrated. To name a few, Madin Darby Canine kidney (MDCKII) cells,[79] human breast cancer cells,[66] human prostate cancer cells and bladder cancer cells,[78] HeLa cells (Figs. 8(a) and 8(b)),[34,41,81,84] HepG2 cells,[72,75,76,83,84] SKOV3 cancer cells,[50] AtT20 cells (Fig. 8(c)),[36,42] Raw 264.7 cells,[74,77,82,83] and A20 lymphoma cells[49] (Fig. 9) were immuno-stained with different long-lived luminescent probes and observed by TG imaging.

Microorganisms such as *Giardia* and *Cryptosporidium* labeled with europium chelate fluorophore markers were visualized against AF background with TG luminescence microscopy,[24,30,32,71,85] as illustrated in Figs. 10(a) and 10(b). Similarly, stained *Daphnia magna* was imaged by TGLI systems.[72,75,82–84] One representative result is shown in Fig. 10(c), where the target probes (hypochlorous acid (HClO)) can be clearly visualized by eliminating strong blue AF from *Daphnia magna*.

4.2. *Tissues*

Tissues labeled with long-lived biocompatible probes revealed by TG imaging would greatly benefit biomedical and clinical applications, such as improved specificity of tumor imaging. In the past few years, TG imaging of tissues (from zebrafishes, mice, to humans) has been extensively investigated.

Because zebrafishes are almost transparent, they are suitable models for fluorescence imaging. TGLI of zebrafish larvae was demonstrated,[20,41,74,81,82] and representative results are shown in Fig. 11. A mouse model has been one of the most common approaches in biological and medical studies. Cubeddu *et al.* utilized TGFI for the detection of tumors in the murine model in 1993.[27] The conditions (e.g., drug doses, delay time in TG imaging, etc.) to optimize fluorescence contrast between the tumor area and the surrounding healthy tissue were studied. In the last decade, TGLI of labeled mouse tissue has attracted much attention.[25,31,35,37,38,43,48,51,77,81,86] For a few examples, Joo *et al.* presented the use of a Si NP probe with lifetime of microseconds for contrast improvement of >100 fold by TGLI (versus CW imaging).[35] Figure 12 shows CW and TG images of mouse tissues (brain, liver, heart, kidney, lung, spleen, and tumor) before and after localized injection of porous Si NPs (PSiNPs) and molecular dyes (AF647). Rosal *et al.* and Liu *et al.* demonstrated similar TG imaging of mouse tissues in some organs and xenograft tumors in mice using different NPs and QDs with long luminescence lifetime to

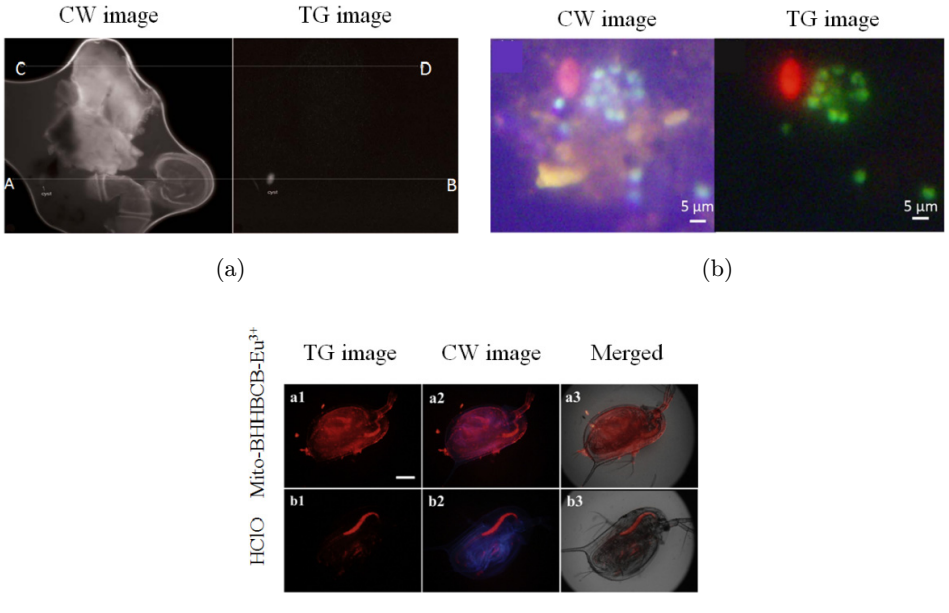

Fig. 10. (a) CW and TG images of *Giardia* cyst labeled with a BHHST (shown on lines A and B) and AF (shown on lines C and D). (b) CW and TG images of *Giardia lamblia* cysts labeled with a red europium probe and *Cryptosporidium parvum* oocysts labeled with a green terbium probe. (c) TG luminescence images of *Daphnia magna* loaded with Mito-BHHBCB-Eu^{3+} for 30 min (top, as control experiment), followed by incubation with HClO for 20 min (bottom) (1: TG image; 2: CW image; 3: merged image of bright field and TG images). Scale bar: 200 μm. Reprinted with permission from Refs. 24, 71 and 83.

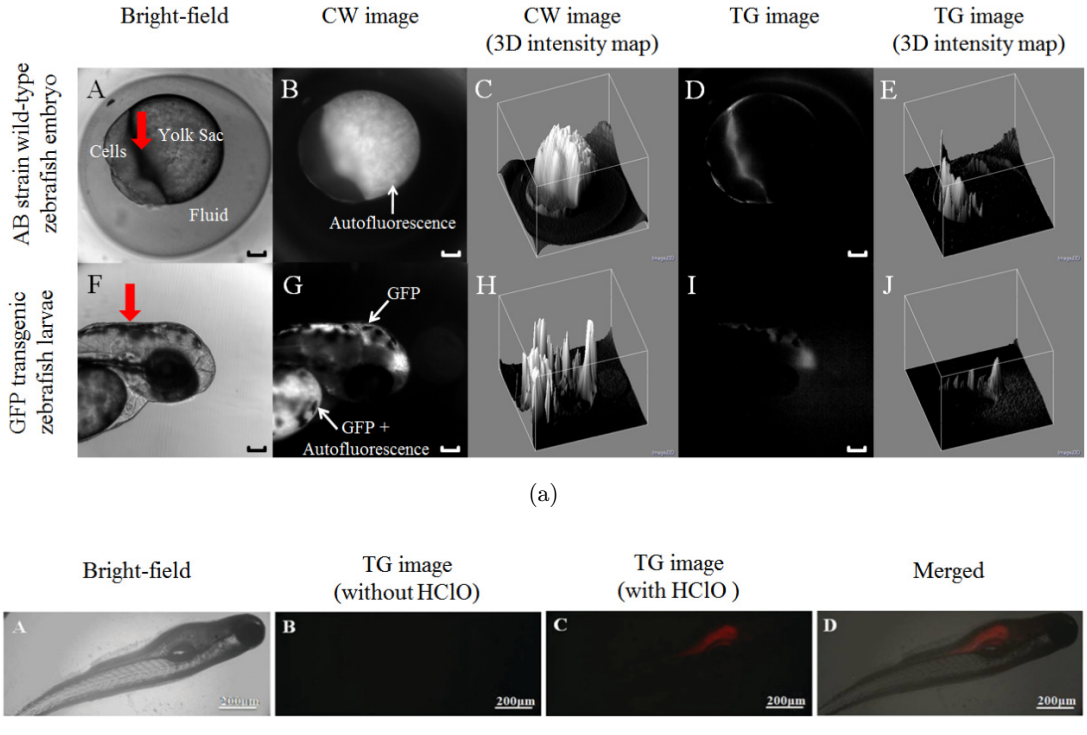

Fig. 11. Comparison of CW and TG images of zebrafish embryos and larvae *in vivo*. (a) Si-based NPs as long-lived fluorescent probes were injected at the position indicated by the red arrow in A and F. Scale bar: 50 μm. (b) Mito-NPSTTA-Eu^{3+} was used as a luminescent probe for TG luminescence detection of HClO in zebrafish larvae. D is merged image of A and C. Reprinted with permission from Refs. 20 and 74.

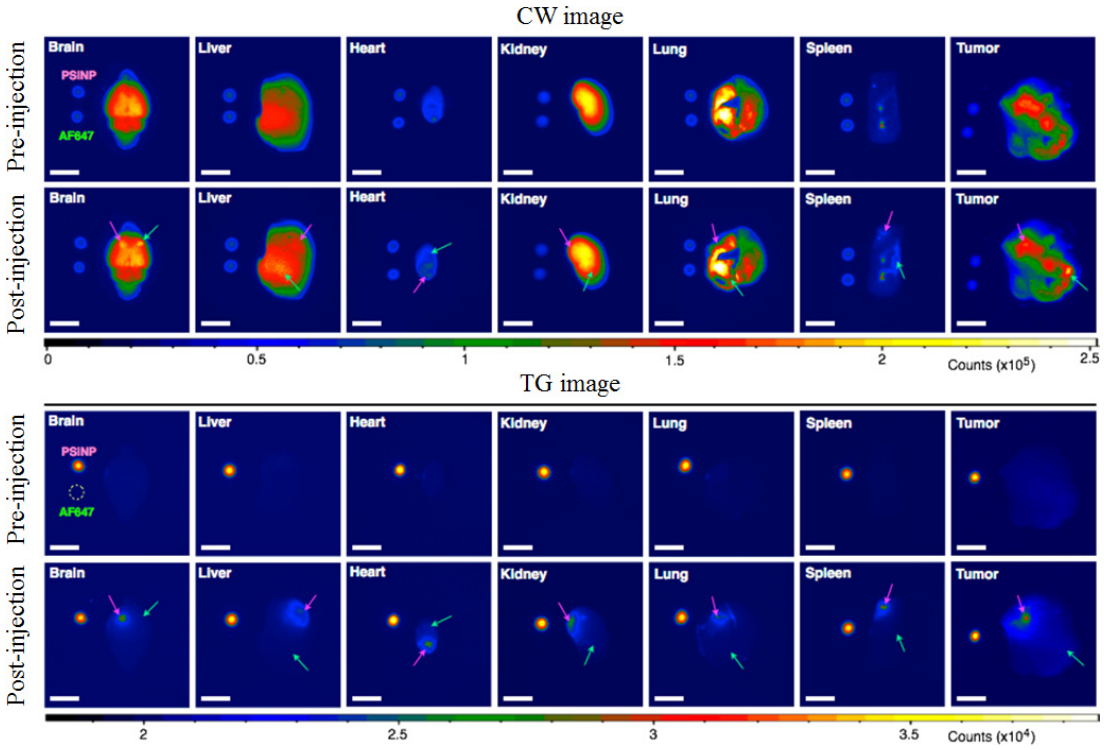

Fig. 12. Comparison of CW and TG images of *ex vivo* mouse tissues before and after localized injection of PSiNPs and AF647. The locations of injection of PSiNPs and AF647 are indicated by pink and green arrows, respectively. The same organs harvested from a 4T1 breast tumor-bearing mouse were imaged by CW and TG modes. PSiNPs can be clearly imaged by TGLI. Scale bar: 5 mm. Reprinted with permission from Ref. 35.

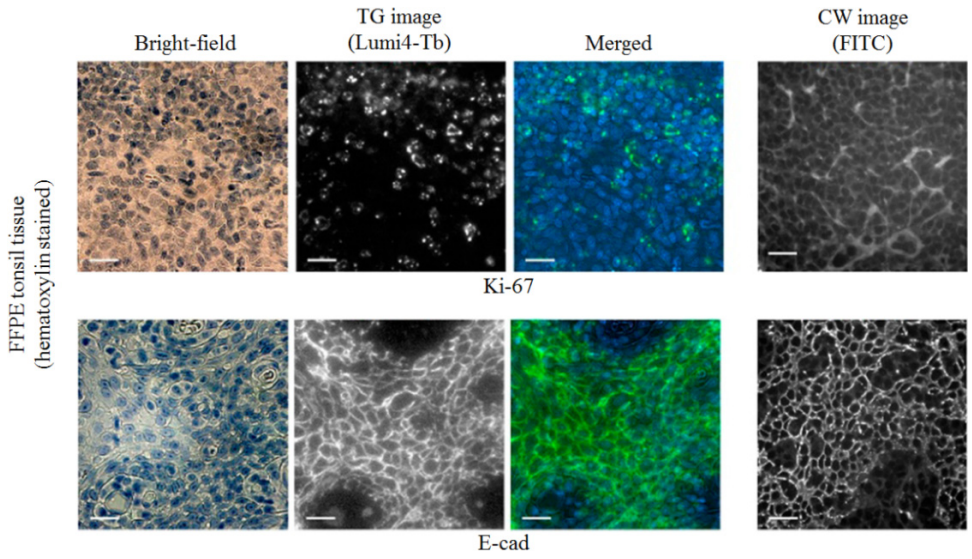

(a)

Fig. 13. (a) FFPE tonsil tissue was stained with hematoxylin, labeled with primary antibodies against Ki-67 (top) or E-cad (bottom), and stained with Lumi4-Tb (TG image) or FITC (CW image) using tyramide signal amplification. Merged images consists of bright-field images (log-transformed into a pseudo-darkfield presentation) and TG images. (b) Tonsil tissue was stained with H&E prior to antigen retrieval, primary antibody labeling (Bcl-6 or MSH-6), and TSA-mediated deposition of Lumi4-Tb or FITC. In these images, robust, specific Lumi4-Tb signals were observed in TG images while FITC signals could not be detected. Scale bars: 20 μm. Reprinted with permission from Ref. 40.

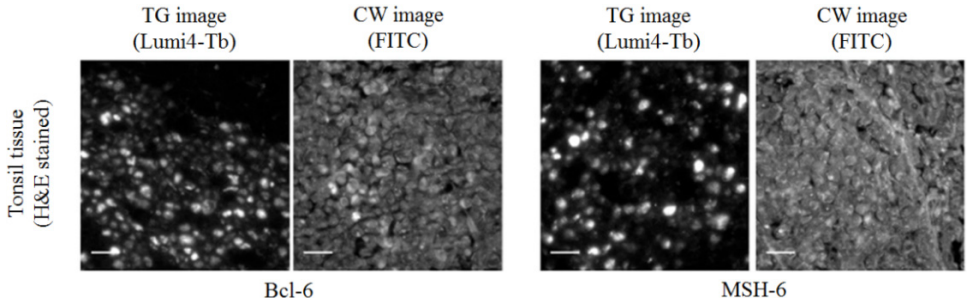

(b)

Fig. 13. (*Continued*)

overcome AF and to show tumor-targeted imaging, respectively.[25,38] Gu *et al.* presented *in vivo* TGLI of human ovarian cancer xenograft in a mouse model, which was labeled with NIR luminescent Si NPs.[86] Very recently, Gu *et al.* have utilized NIR-excited upconversion nanoprobes with high-light conversion efficiency to achieve high-sensitivity deep-tissue TG imaging in a mouse tumor model.[51]

TG imaging of human tissue has also been reported. Chen *et al.* demonstrated TGLI of human tonsil tissue.[40] Briefly, Lumi4-Tb-conjugated antibodies were used to visualize various markers including Ki-67 (nucleus), E-cad (membrane), Bcl-6, and MSH-6. TG imaging provides higher contrast than CW imaging owing to the elimination of AF background, as shown in Fig. 13. Figure 13(b) shows strong TG luminescence signals of Lumi4-Tb with antibody binding (Bcl-6 or MSH-6) for specimens stained with H&E (the primary stain for cancer diagnosis).

5. Conclusions

Rapid development of TGFI techniques facilitates the utilization of long-lived luminescent probes for biological analysis and imaging applications, which overcomes the issue due to complicated tissue environment. The key advantage of TG imaging is that it selectively detects long-lived luminescence signals from probes by delayed detection after the termination of excitation, which leads to high-contrast imaging by eliminating interference of short-lived AF. In recent years, the performance of the technique has been remarkably improved by the technical advances of excitation light sources and detection imagers. Various TG implementation methods and progress based on optical choppers and electronic units were reviewed. The performance and cost of TG imaging systems are always a trade-off and have to be balanced. Besides, recent advances in TGFI biological applications were also described. It is believed that further development of TG imaging technology as well as more related biological studies would pave the way toward future clinical translation of TGFI.

Acknowledgment

This research was supported by National Natural Science Foundation (NSFC) (Grant No. 61775134).

References

1. E. J. Soini, L. J. Pelliniemi, I. A. Hemmilä, V. M. Mukkala, J. J. Kankare, K. Fröjdman, "Lanthanide chelates as new fluorochrome labels for cytochemistry," *J. Histochem. Cytochem.* **36**(11), 1449–1451 (1988).
2. S. Andersson-Engels, C. af Klinteberg, K. Svanberg, S. Svanberg, "*In vivo* fluorescence imaging for tissue diagnostics," *Phys. Med. Biol.* **42**(5), 815 (1997).
3. J. V. Frangioni, "*In vivo* near-infrared fluorescence imaging," *Curr. Opin. Chem. Biol.* **7**(5), 626–634 (2003).
4. T. Terai, T. Nagano, "Fluorescent probes for bioimaging applications," *Curr. Opin. Chem. Biol.* **12** (5), 515–521 (2008).
5. U. Resch-Genger, M. Grabolle, S. Cavaliere-Jaricot, R. Nitschke, T. Nann, "Quantum dots versus organic dyes as fluorescent labels," *Nat. Meth.* **5**(9), 763 (2008).
6. F. Leblond, S. C. Davis, P. A. Valdés, B. W. Pogue, "Pre-clinical whole-body fluorescence imaging: Review of instruments, methods and applications," *J. Photochem. Photobiol. B. Biol.* **98**(1), 77–94 (2010).

7. M. V. Marshall, J. C. Rasmussen, I. C. Tan, M. B. Aldrich, K. E. Adams, X. Wang, E. M. Sevick-Muraca, "Near-infrared fluorescence imaging in humans with indocyanine green: A review and update," *Open Surg. Oncol. J. (Online)*, **2**(2), 12 (2010).
8. S. Bouccara, G. Sitbon, A. Fragola, V. Loriette, N. Lequeux, T. Pons, "Enhancing fluorescence *in vivo* imaging using inorganic nanoprobes," *Curr. Opin. Biotechnol.* **34**, 65–72 (2015).
9. K. Y. Zhang, Q. Yu, H. Wei, S. Liu, Q. Zhao, W. Huang, "Long-lived emissive probes for time-resolved photoluminescence bioimaging and biosensing," *Chem. Rev.* **118**(4), 1770–1839 (2018).
10. B. Del Rosal, A. Benayas, "Strategies to overcome autofluorescence in nanoprobe-driven *in vivo* fluorescence imaging," *Small Meth.* **2**(9), 1800075 (2018).
11. G. Marriott, R. M. Clegg, D. J. Arndt-Jovin, T. M. Jovin, "Time resolved imaging microscopy. Phosphorescence and delayed fluorescence imaging," *Biophys. J.* **60**(6), 1374–1387 (1991).
12. G. Vereb, E. Jares-Erijman, P. R. Selvin, T. M. Jovin, "Temporally and spectrally resolved imaging microscopy of lanthanide chelates," *Biophys. J.* **74**(5), 2210–2222 (1998).
13. R. Cubeddu, D. Comelli, C. D'Andrea, P. Taroni, G. Valentini, "Time-resolved fluorescence imaging in biology and medicine," *J. Phys. D. Appl. Phys.* **35**(9), R61 (2002).
14. R. E. Connally, J. A. Piper, "Time-gated luminescence microscopy," *Ann. New York Acad. Sci.* **1130**(1), 106–116 (2008).
15. J. R. Lakowicz, Introduction to fluorescence, *Principles of Fluorescence Spectroscopy*, Springer, Boston, MA (1999).
16. J. R. Lakowicz, Time-domain lifetime measurements, *Principles of Fluorescence Spectroscopy*, Springer, Boston, MA (1999).
17. B. Valeur, "Molecular fluorescence," *Digital Encyclopedia Appl. Phys.* 477–531 (2003).
18. N. Boens, W. Qin, N. Basarić, J. Hofkens, M. Ameloot, J. Pouget, N. D. Silva, "Fluorescence lifetime standards for time and frequency domain fluorescence spectroscopy," *Anal. Chem.* **79**(5), 2137–2149 (2007).
19. F. Menezes, A. Fedorov, C. Baleizao, B. Valeur, M. N. Berberan-Santos, "Methods for the analysis of complex fluorescence decays: Sum of Becquerel functions versus sum of exponentials," *Meth. Appl. Fluores.* **1**(1), 015002 (2013).
20. Y. Lu, M. Abran, G. Cloutier, F. Lesage, Catheter-based time-gated near-infrared fluorescence/OCT imaging system, *Diagnostic and Therapeutic Applications of Light in Cardiology, Int. Society for Optics and Photonics*, Vol. 10471 (SPIE BiOS, San Francisco, California, United States, 2018) pp. 104710D-1–7.
21. S. V. Eliseeva, J. C. G. Bünzli, "Lanthanide luminescence for functional materials and bio-sciences," *Chem. Soc. Rev.* **39**(1), 189–227 (2010).
22. P. Hänninen, H. Härmä (Eds.)., *Lanthanide Luminescence: Photophysical, Analytical and Biological Aspects*, Springer Science & Business Media, Vol. 7 (2011).
23. G. Marriott, M. Heidecker, E. P. Diamandis, Y. Yan-Marriott, "Time-resolved delayed luminescence image microscopy using an europium ion chelate complex," *Biophys. J.* **67**(3), 957–965 (1994).
24. R. E. Connally, J. A. Piper, "Solid-state time-gated luminescence microscope with ultraviolet light-emitting diode excitation and electron-multiplying charge-coupled device detection," *J. Biomed. Opt.* **13**(3), 034022 (2008).
25. B. Del Rosal, D. H. Ortgies, N. Fernández, F. Sanz-Rodríguez, D. Jaque, E. M. Rodríguez, "Overcoming autofluorescence: Long-lifetime infrared nanoparticles for time-gated *in vivo* imaging," *Adv. Mater.* **28**(46), 10188 (2016).
26. X. F. Wang, T. Uchida, D. M. Coleman, S. Minami, "A two-dimensional fluorescence lifetime imaging system using a gated image intensifier," *Appl. Spectrosc.* **45**(3), 360–366 (1991).
27. R. Cubeddu, G. Canti, P. Taroni, G. Valentini, "Time-gated fluorescence imaging for the diagnosis of tumors in a murine model," *Photochem. Photobiol.* **57**(3), 480–485 (1993).
28. G. Valentini, C. D'Andrea, D. Comelli, A. Pifferi, P. Taroni, A. Torricelli, L. Rossi-Bernardi, "Time-resolved DNA-microarray reading by an intensified CCD for ultimate sensitivity," *Opt. Lett.* **25**(22), 1648–1650 (2000).
29. M. Dahan, T. Laurence, F. Pinaud, D. S. Chemla, A. P. Alivisatos, M. Sauer, S. Weiss, "Time-gated biological imaging by use of colloidal quantum dots," *Opt. Lett.* **26**(11), 825–827 (2001).
30. R. Connally, D. Jin, J. Piper, "High intensity solid-state UV source for time-gated luminescence microscopy," *Cytometr. A. J. Int. Soc. Anal. Cytol.* **69**(9), 1020–1027 (2006).
31. A. May, S. Bhaumik, S. S. Gambhir, C. Zhan, S. Yazdanfar, "Whole-body, real-time preclinical imaging of quantum dot fluorescence with time-gated detection," *J. Biomed. Opt.*, **14**(6), 060504 (2009).
32. D. Jin, J. A. Piper, "Time-gated luminescence microscopy allowing direct visual inspection of lanthanide-stained microorganisms in background-free condition," *Anal. Chem.* **83**(6), 2294–2300 (2011).

33. W. Mo, D. J. Rohrbach, U. Sunar, "Imaging a photodynamic therapy photosensitizer *in vivo* with a time-gated fluorescence tomography system," *J. Biomed. Opt.* **17**(7), 071306 (2012).
34. S. Bouccara, A. Fragola, E. Giovanelli, G. Sitbon, N. Lequeux, T. Pons, V. Loriette, "Time-gated cell imaging using long lifetime near-infrared-emitting quantum dots for autofluorescence rejection," *J. Biomed. Opt.* **19**(5), 051208 (2014).
35. J. Joo, X. Liu, V. R. Kotamraju, E. Ruoslahti, Y. Nam, M. J. Sailor, "Gated luminescence imaging of silicon nanoparticles," *ACS Nano*, **9**(6), 6233–6241 (2015).
36. W. A. Razali, V. K. Sreenivasan, C. Bradac, M. Connor, E. M. Goldys, A. V. Zvyagin, "Wide-field time-gated photoluminescence microscopy for fast ultrahigh-sensitivity imaging of photoluminescent probes," *J. Biophoton.* **9**(8), 848–858 (2016).
37. X. Zheng, X. Zhu, Y. Lu, J. Zhao, W. Feng, G. Jia, D. Jin, "High-contrast visualization of upconversion luminescence in mice using time-gating approach," *Anal. Chem.* **88**(7), 3449–3454 (2016).
38. X. Liu, G. B. Braun, H. Zhong, D. J. Hall, W. Han, M. Qin, M. J. Sailor, "Tumor-targeted multimodal optical imaging with versatile cadmium-free quantum dots," *Adv. Funct. Mater.* **26**(2), 267–276 (2016).
39. C. C. Tu, K. Awasthi, K. P. Chen, C. H. Lin, M. Hamada, N. Ohta, Y. K. Li, "Time-gated imaging on live cancer cells using silicon quantum dot nanoparticles with long-lived fluorescence," *ACS Photon.* **4**(6), 1306–1315 (2017).
40. T. Chen, R. Hong, D. Magda, C. Bieniarz, L. Morrison, L. W. Miller, "Time gated luminescence imaging of immunolabeled human tissues," *Anal. Chem.* **89**(23), 12713–12719 (2017).
41. T. Li, D. Yang, L. Zhai, S. Wang, B. Zhao, N. Fu, W. Huang, "Thermally activated delayed fluorescence organic dots (TADF Odots) for time-resolved and confocal fluorescence imaging in living cells and *in vivo*," *Adv. Sci.* **4**(4), 1600166 (2017).
42. V. K. Sreenivasan, Wan Razali, W. A., K. Zhang, R. R. Pillai, A. Saini, D. Denkova, E. M. Goldys, "Development of bright and biocompatible nanoruby and its application to background-free time-gated imaging of G-protein-coupled receptors," *ACS Appl. Mater. Interf.* **9**(45), 39197–39208 (2017).
43. P. Sawosz, S. Wojtkiewicz, M. Kacprzak, E. Zieminska, M. Morawiec, R. Maniewski, A. Liebert, "Towards *in-vivo* assessment of fluorescence lifetime: imaging using time-gated intensified CCD camera," *Biocybernet. Biomed. Eng.* **38**(4), 966–974 (2018).
44. M. Sakiyama, H. Sugimoto, M. Fujii, "Long-lived luminescence of colloidal silicon quantum dots for time-gated fluorescence imaging in the second near infrared window in biological tissue," *Nanoscale*, **10**(29), 13902–13907 (2018).
45. Z. Zhu, D. Tian, X. Shu, "Auto-phase-locked time-gated luminescence detection for background-free upconversion spectra measurement and true-color biological imaging," *Sens. Actuators B. Chem.* **260**, 289–294 (2018).
46. S. Shkolyar, E. J. Eshelman, J. D. Farmer, D. Hamilton, M. G. Daly, C. Youngbull, "Detecting kerogen as a biosignature using colocated UV time-gated Raman and fluorescence spectroscopy," *Astrobiol.*, **18**(4), 431–453 (2018).
47. R. Chib, S. Requena, M. Mummert, Y. M. Strzhemechny, I. Gryczynski, J. Borejdo, R. Fudala, "Fluorescence lifetime imaging with time-gated detection of hyaluronidase using a long lifetime azadioxatriangulenium (ADOTA) fluorophore," *Meth. Appl. Fluorescence*, **4**(4), 047001 (2016).
48. S. Cheng, B. Shen, W. Yuan, X. Zhou, Q. Liu, M. Kong, F. Li, "Time-gated ratiometric detection with the same working wavelength to minimize the interferences from photon attenuation for accurate *in vivo* detection," *ACS Central Sci.* **5**(2), 299–307 (2019).
49. T. Pons, S. Bouccara, V. Loriette, N. Lequeux, S. Pezet, A. Fragola, "*In vivo* imaging of single tumor cells in fast-flowing bloodstream using near-infrared quantum dots and time-gated imaging," *ACS Nano*, **13**(3), 3125–3131 (2019).
50. X. D. Chen, Y. Zheng, B. Du, D. F. Li, S. Li, Y. Dong, G.-C. Guo, F. W. Sun, "High-contrast quantum imaging with time-gated fluorescence detection," *Phys. Rev. Appl.* **11**(6), 064024 (2019).
51. Y. Gu, Z. Guo, W. Yuan, M. Kong, Y. Liu, Y. Gao, W. Feng, F. Wang, J. Zhou, D. Jin, F. Li, "High-sensitivity imaging of time-domain near-infrared light transducer," *Nat. Photon.* (2019).
52. Z. Zhu, X. Shu, "Global luminescence lifetime imaging of thermally activated delayed fluorescence on an auto-phase-locked time-gated microscope," *Sens. Actuators B. Chem.* **280**, 177–182 (2019).
53. H. Kume, S. Suzuki, J. Takeuchi, K. Oba, "Newly developed photomultiplier tubes with position sensitivity capability," *IEEE Trans. Nucl. Sci.*, **32**(1), 448–452 (1985).
54. K. H. Kim, C. Buehler, K. Bahlmann, T. Ragan, W. C. A. Lee, E. Nedivi, E. L. Heffer, S. Fantini, P. T. C. So, "Multifocal multiphoton microscopy based on multianode photomultiplier tubes," *Opt. Exp.* **15**(18), 11658–11678 (2007).
55. M. Caccia, L. Nardo, R. Santoro, D. Schaffhauser, "Silicon photomultipliers and SPAD imagers in biophotonics: advances and perspectives," *Nucl. Instrum. Meth. Phys. Res. A. Accel. Spectrom. Detect. Assoc. Equip.* **926**, 101–117 (2018).

56. L. Pancheri, D. Stoppa, "A SPAD-based pixel linear array for high-speed time-gated fluorescence lifetime imaging," *2009 Proc. ESSCIRC* (IEEE, Athens, Greece, 2009), pp. 428–431.
57. L. Pancheri, N. Massari, D. Stoppa, "SPAD image sensor with analog counting pixel for time-resolved fluorescence detection," *IEEE Trans. Electron Dev.* **60**(10), 3442–3449 (2013).
58. A. C. Ulku, C. Bruschini, S. Weiss, X. Michalet, E. Charbon, "A time-gated large-array SPAD camera for picosecond resolution real-time FLIM," *Multiphoton Microscopy in the Biomedical Sciences XVIII*, Vol. 10498, International Society for Optics and Photonics (SPIE BiOS, San Francisco, California, United States, 2018), p. 104980M.
59. I. Gyongy, A. Green, S. W. Hutchings, A. Davies, N. A. Dutton, R. R. Duncan, C. Rickman, R. K. Henderson, P. A. Dalgarno, Fluorescence lifetime imaging of high-speed particles with single-photon image sensors, *High-Speed Biomedical Imaging and Spectroscopy IV*, Vol. 10889, p. 108890O, International Society for Optics and Photonics (2019).
60. M. Perenzoni, N. Massari, D. Perenzoni, L. Gasparini, D. Stoppa, "A 160X120 pixel analog-counting single-photon imager with time-gating and self-referenced column-parallel A/D conversion for fluorescence lifetime imaging," *IEEE J. Solid-State Circuit.* **51**(1), 155–167 (2015).
61. W. Becker, B. Su, O. Holub, K. Weisshart, "FLIM and FCS detection in laser-scanning microscopes: Increased efficiency by GaAsP hybrid detectors," *Microscopy Res. Techniq.* **74**(9), 804–811 (2011).
62. D. Kim, W. Hwang, Y. Won, S. Moon, S. Y. Lee, M. Kang, W. S. Han, D. Y. Kim, "Enhancement of performance in time-domain FLIM with GaAsP hybrid detectors," *Multiphoton Microscopy in the Biomedical Sciences XIX*, International Society for Optics and Photonics, Vol. 10882 (SPIE BiOS, San Francisco, California, United States, 2019), pp. 108821J-1–4.
63. T. Lapauw, H. Ingelberts, T. Van den Dries, M. Kuijk, Sub-nanosecond time-gated camera based on a novel current-assisted CMOS image sensor, *Photonic Instrumentation Engineering VI*, International Society for Optics and Photonics, Vol. 10925 (SPIE OPTO, San Francisco, California, United States, 2019), pp. 1092506-1–9.
64. D. Elson, J. Requejo-Isidro, I. Munro, F. Reavell, J. Siegel, K. Suhling, P. Tadrous, R. Benninger, P. Lanigan, J. McGinty, C. Talbot, B. Treanor, S. Webb, A. Sandison, A. Wallace, D. Davis, J. Lever, M. Neil, D. Phillips, G. Stampa, P. Frencha, "Time-domain fluorescence lifetime imaging applied to biological tissue," *Photochem. Photobiol. Sci.* **3**(8), 795–801 (2004).
65. K. Suhling, P. M. French, D. Phillips, "Time-resolved fluorescence microscopy," *Photochem. Photobiol. Sci.* **4**(1), 13–22 (2005).
66. Y. AndrewáWang, "Cadmium-free quantum dots as time-gated bioimaging probes in highly-auto-fluorescent human breast cancer cells," *Chem. Commun.* **49**(6), 624–626 (2013).
67. S. Lindén, M. K. Singh, K. D. Wegner, M. Regairaz, F. Dautry, F. Treussart, N. Hildebrandt, "Terbium-based time-gated Förster resonance energy transfer imaging for evaluating protein-protein interactions on cell membranes," *Dalton Trans.* **44**(11), 4994–5003 (2015).
68. M. C. Dos Santos, N. Hildebrandt, "Recent developments in lanthanide-to-quantum dot FRET using time-gated fluorescence detection and photon upconversion," *Trends Anal. Chem.* **84**, 60–71 (2016).
69. C. Chen, L. Ao, Y. T. Wu, V. Cifliku, M. Cardoso Dos Santos, E. Bourrier, M. Delbianco, D. Parker, J. M. Zwier, L. Huang, N. Hildebrandt, "Single-nanoparticle cell barcoding by tunable FRET from lanthanides to quantum dots," *Angewandte Chemie Int. Edn.* **57**(41), 13686–13690 (2018).
70. H. B. Beverloo, A. Van Schadewijk, S. van Gelderen-Boele, H. J. Tanke, "Inorganic phosphors as new luminescent labels for immunocytochemistry and time-resolved microscopy," *Cytometry. J. Int. Soc. Anal. Cytol.* **11**(7), 784–792 (1990).
71. L. Zhang, X. Zheng, W. Deng, Y. Lu, S. Lechevallier, Z. Ye, E. M. Goldys, J. M. Dawes, J. A. Piper, J. Yuan, M. Verelst, D. Jin, "Practical implementation, characterization and applications of a multi-colour time-gated luminescence microscope," *Sci. Rep.* **4**, 6597 (2014).
72. B. Song, Z. Ye, Y. Yang, H. Ma, X. Zheng, D. Jin, J. Yuan, "Background-free in-vivo imaging of vitamin C using time-gateable responsive probe," *Sci. Rep.*, **5**, 14194 (2015).
73. R. Connally, "A device for gated autosynchronous luminescence detection," *Anal. Chem.* **83**(12), 4782–4787 (2011).
74. X. Liu, Z. Tang, B. Song, H. Ma, J. Yuan, "A mitochondria-targeting time-gated luminescence probe for hypochlorous acid based on a europium complex," *J. Mater. Chem. B.* **5**(15), 2849–2855 (2017).
75. Z. Dai, L. Tian, B. Song, X. Liu, J. Yuan, "Development of a novel lysosome-targetable time-gated luminescence probe for ratiometric and luminescence lifetime detection of nitric oxide *in vivo*," *Chem. Sci.* **8**(3), 1969–1976 (2017).
76. Y. Wang, H. Wang, X. Zhao, Y. Jin, H. Xiong, J. Yuan, J. Wu, "A β-diketonate–europium (III) complex-based fluorescent probe for highly sensitive

time-gated luminescence detection of copper and sulfide ions in living cells," *New J. Chem.* **41**(13), 5981–5987 (2017).

77. Z. Dai, H. Ma, L. Tian, B. Song, M. Tan, X. Zheng, J. Yuan, "Construction of a multifunctional nanoprobe for tumor-targeted time-gated luminescence and magnetic resonance imaging in vitro and *in vivo*," *Nanoscale* **10**(24), 11597–11603 (2018).
78. N. Sayyadi, I. Justiniano, R. E. Connally, R. Zhang, B. Shi, L. Kautto, A. V. Everest-Dass, J. Yuan, B. J. Walsh, D. Jin, R. D. Willows, J. A. Piper, N. H. Packer, "Sensitive time-gated immunoluminescence detection of prostate cancer cells using a TEGylated europium ligand," *Anal. Chem.* **88**(19), 9564–9571 (2016).
79. N. Gahlaut, L. W. Miller, "Time-resolved microscopy for imaging lanthanide luminescence in living cells," *Cytometry A* **77**(12), 1113–1125 (2010).
80. M. Rosenberg, K. R. Rostgaard, Z. Liao, A. Ø. Madsen, K. L. Martinez, T. Vosch, B. W. Laursen, "Design, synthesis, and time-gated cell imaging of carbon-bridged triangulenium dyes with long fluorescence lifetime and red emission," *Chem. Sci.* **9**(12), 3122–3130 (2018).
81. B. Song, W. Shi, W. Shi, X. Qin, H. Ma, M. Tan, W. Zhang, L. Guo, J. Yuan, "A dual-modal nanoprobe based on Eu (iii) complex-MnO 2 nanosheet nanocomposites for time-gated luminescence–magnetic resonance imaging of glutathione in vitro and *in vivo*," *Nanoscale* **11**(14), 6784–6793 (2019).
82. H. Ma, B. Song, Y. Wang, D. Cong, Y. Jiang, J. Yuan, "Dual-emissive nanoarchitecture of lanthanide-complex-modified silica particles for *in vivo* ratiometric time-gated luminescence imaging of hypochlorous acid," *Chem. Sci.* **8**(1), 150–159 (2017).
83. H. Ma, B. Song, Y. Wang, C. Liu, X. Wang, J. Yuan, "Development of organelle-targetable europium complex probes for time-gated luminescence imaging of hypochlorous acid in live cells and animals," *Dyes Pigments* **140**, 407–416 (2017).
84. Q. Gao, W. Zhang, B. Song, R. Zhang, W. Guo, J. Yuan, "Development of a novel lysosome-targeted ruthenium (II) complex for phosphorescence/time-gated luminescence assay of biothiols," *Anal. Chem.* **89**(8), 4517–4524 (2017).
85. D. Jin, R. Connally, J. Piper, "Practical time-gated luminescence flow cytometry. II: Experimental evaluation using UV LED excitation," *Cytometry A. J. Int. Soc. Anal. Cytol.* **71**(10), 797–808 (2007).
86. L. Gu, D. J. Hall, Z. Qin, E. Anglin, J. Joo, D. J. Mooney, S. B. Howell, M. J. Sailor, "*In vivo* time-gated fluorescence imaging with biodegradable luminescent porous silicon nanoparticles," *Nat. Commun.* **4**, 2326 (2013).